MECH 436-Control Systems

Instructor: Prof. Dany Abou Jaoude

Spring 2021

Course Project

Closed-Loop Control for Propofol Delivery

Group Members:

Hadi Hammoud 201803281

Sari Tarabay 201901345

Jad Dika 201804975

Abstract

Anesthetic drugs are traditionally administered manually by a medical professional or, more recently, with the assistance of computer-aided systems. This paper aims to explore a more sophisticated approach to anesthetic drug ingestion, namely consisting of a fully automated closed-loop drug delivery system. Several clinical studies have shown that such systems have the potential of decreasing drug dosage, patient recovery time, and workload in the anesthesiologist while promoting the safety of the patient. However, such as system must be robustly designed in order to account for the effect of interpatient variability in drug response. In this paper, we consider a simplified model for the clinical effect of propofol, an anesthetic, and describe the process of experimentally identifying such a model based on its frequency response. We then present two controller designs, a Lag-Lead compensator and a PID compensator, to be used in conjunction with this model in a closed-loop setup. We found that such a system can be designed in compliance with performance and steady-state error requirements. Nevertheless, the system was designed and simulated in an idealized environment implying it is still far from practical implementation.

Table of Contents

List Of Figures

Introduction

Anesthesia is the process of inducing a patient into a state of temporary unconsciousness and insensitivity to pain necessary for the performance of surgery. The patient is put into this state thanks to the effect of special drugs called anesthetics. Propofol is a commonly employed intravenously administered anesthetic that is usually used in combination with opioids, such as remifentanil. The process of administering anesthetics such as propofol should be done with care; overdosing might be lethal to the patient while underdosing may leave the patient sensitive to pain during surgery. In this paper, we are interested in investigating a relatively novel approach to propofol administration, namely, we explore the possibility of implementing an automated closed-loop propofol delivery system. In this respect, we start by reviewing the literature concerned with traditional approaches to anesthesia, along with more advanced computer aided delivery systems based on mathematical modeling, to later look at several proposed designs for closed-loop drug administration systems. In the next part of the paper, we present our own approach for implementing such a closed-loop system. We start by describing the preliminary system identification task required to obtain an open-loop model for the clinical effect of propofol. We later present our designs for two types of controllers, a Lag-Lead controller and a PID controller, to be employed in closed-loop propofol delivery systems.

1. Literature Review

1.1 Conventional Propofol Delivery Protocols

Traditionally, hypnotic drugs like propofol are administered by a professional anesthetist. The anesthetist directly controls the propofol flow, which is supplied by an infusion pump through an intravenous line [1],[4],[6],[7]. Evidently, the patient needs to be under the effect of the anesthesia over the whole course of the surgery; this requires the continuous maintenance of propofol infusion. The latter is ensured by the anesthetist, who closely monitors the propofol flow rate and adjusts it based on the observation of the patient's state [4],[6],[7]. This state is inferred from both quantitatively measured signals, such as heart rate blood pressure and oxygen saturation, and qualitative signs, such as movements or sudden reflexes [4].

A more direct measure of the degree to which the patient is under the effect of the anesthetic is given by the Depth of Hypnosis (DOH), which consists of a quantitative indicator calculated based on the patient's cerebral activity monitored by an Electroencephalogram (EEG) [1], [3]-[7]. The DOH is a value ranging from 0 to 1 (or 0-100%); a DOH ranging from 0.9 to 1 corresponds to an awake state while a value of 0 corresponds to a complete loss of brain activity; the DOH range corresponding to a stable anesthetic condition suitable for surgery is from 0.4 to 0.6 [5],[6].

Various DOH monitors exist, but the most widely used is the Bispectral Index (BIS) monitor; the BIS being one of several DOH indices bearing the same significance [1],[3],[4],[6]. The anesthetist can thus keep track of the patient's response by monitoring BIS measurements displayed on the graphical interface of the monitor to adjust the propofol flow rate accordingly. Consequently, this continuous observation and regulation process puts a significant workload on the anesthetist which may lead to dosing errors that could threaten the patient's life [4].

More sophisticated propofol administration techniques employ computer-controlled infusion pumps to deliver the drug. Instead of manually adjusting the propofol flow rate, the anesthetist can directly specify a desired propofol plasma concentration based on the observation of the patient's state. The latter is fed to a computer software, controlling the infusion pump, that would calculate then dictate the appropriate infusion profile, or infusion rates, corresponding to the target concentration; this method is known as Target Controlled Infusion (TCI) [1],[3],[4],[6],[7].

In order to correctly estimate infusion rates that would lead to achieving a specific propofol blood concentration level, mathematical models relating these two quantities are required. Several such models exist, and they are all based on Pharmacokinetic[1] (PK) theory [1],[3]-[7]; these models will be discussed in more detail in the subsequent section. This open-loop control scheme offers the anesthetist more control over drug dosage, thus reducing errors and relieving workload [4].

Nevertheless, TCI has some limitations; this is mainly due to the unavailability of propofol concentration measurements during surgery, which prevents the anesthetist from obtaining useful feedback and necessitates extremely accurate PK models [1],[4]. Also, like any other open-loop control system, TCI is prone to model-error and sensitive to disturbances [4], [6]. We should also note that although TCI is a widely used propofol administration technique, its use in children surgery is still debated due to the large interpatient variability of PK behavior in children [4], [7].

[1] Pharmacokinetics describe the transport and metabolism of a drug in the human body.

1.2 Closed-Loop Propofol Delivery Systems

In an attempt to optimize the propofol administration procedure, it has been suggested to introduce a closed-loop control scheme that would fully automate the drug infusion and maintenance processes [1]-[7]. Specifically, this scheme relies on feedback from DOH monitors to continuously control the drug infusion rates until a suitable DOH value specified by the medical professional is achieved [1]-[7]. Clearly, the latter cannot be achieved without a full understanding of the correlation between the propofol infusion rates and the patient's clinical state reflected by the DOH.

1.2.1 Open-Loop Model Structure

The effect of propofol on the DOH is described by Pharmacokinetic-Pharmacodynamic[2] (PKPD) models [1],[3]-[7]; there exists several such models that have the same overall structure that we shall now discuss. The PK model relates the propofol infusion rate $u(t)$ to its plasma concentration $C_p(t)$ and it generally consists of a third-order Linear Time-Invariant (LTI) system [1],[4],[6],[7]. The model can be represented by the following transfer function in the general form [1]:

$$PK(s) = \frac{C_p(s)}{U(s)} = \frac{1}{V_1}\frac{(s+z_1)(s+z_2)}{(s+p_1)(s+p_2)(s+p_3)} \tag{1}$$

As for the PD model, it describes the relationship between $C_p(t)$ and the drug's clinical effect on the patient $E(t)$ which is quantified by the DOH [1],[4],[6],[7]. In contrast to the PK model, the PD model is a non-linear First Order Time Delayed (FOTD) model. In particular, the PD model first relates the propofol plasma concentration $C_p(t)$ to the effect site concentration[3] $C_e(t)$ by a

[2] Pharmacodynamics describe the relationship between drug concentration and their clinical effect.
[3] Effect site concentration is the concentration of a drug at the site of its biological activity.

FOTD model involving a term representing response time delay. $C_e(t)$ is then related to the clinical effect $E(t)$ by a non-linear Hill function [1],[4],[6],[7]. The mathematical representation of the FOTD part of the PD model is given by the following transfer function [6]:

$$\frac{C_e(s)}{C_p(s)} = \frac{k_d}{s + k_d} e^{-T_d s} \tag{2}$$

Where the term $e^{-T_d s}$ represents a time delay of T_d. As for the Hill sigmoid, it is given by [6]:

$$\mathrm{E(t)} = \mathrm{E_0} - \mathrm{E_0} \frac{\mathrm{C_e^{\gamma}(t)}}{\mathrm{EC_{50}^{\gamma} + C_e^{\gamma}(t)}} \tag{3}$$

Where E_0 is the initial clinical effect prior to the infusion, EC_{50} is the half-maximal effective drug concentration and the parameter γ determines the non-linearity. A block diagram representation of the combined PKPD model is provided in Figure 1 below.

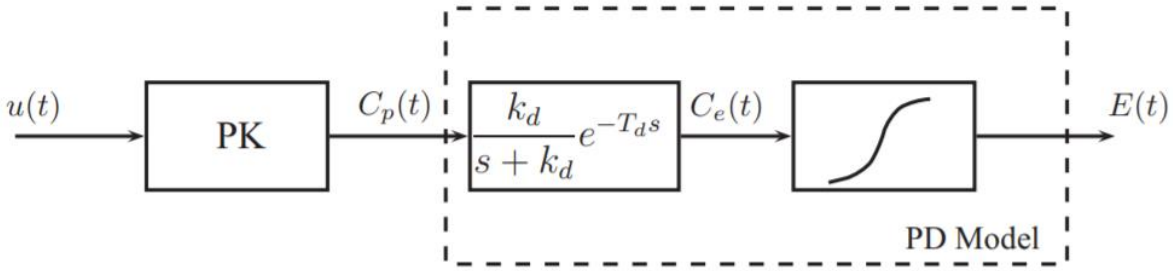

Figure 1: PKPD Model Structure (adapted from [6] and [7])

During surgery, the patient's clinical state is affected by surgical stimulation; the latter is incorporated into the PKPD as modeled by a disturbance $d(t)$ affecting the system [1],[4],[6],[7]. Finally, the clinical state of the patient is measured by a DOH monitor. As mentioned before, the BIS monitor is the most widely used EEG-based monitor. However, it turns out that this monitor

is not suitable for use in closed-loop control as it suffers from several limitations mainly due to its non-linear dynamics and response time delays [1],[4],[7]. A better alternative having LTI dynamics with no time delays was developed specifically for the purposes of closed-loop anesthetic delivery, namely the NeuroSENSE monitor [1],[4],[6],[7]. Instead of the BIS, the NeuroSENSE quantifies the DOH by the WAV_{CNS}[4] index [1],[4],[6],[7]. A zero-mean measurement noise disturbance $n(t)$ is added to the input of the DOH monitor to complete the system's open-loop model [1],[4],[6],[7]. To eliminate this high frequency noise, the NeuroSENSE monitor is equipped with a low-pass trending filter having a known transfer function [1],[4],[6]. The block diagram representation of the system is provided in Figure 2 below. As a final note, we should say that the infusion pump is assumed to have negligible dynamics in all models found in literature [4],[7].

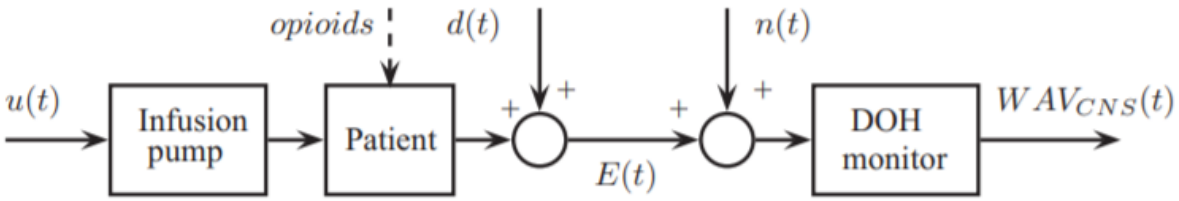

Figure 2: Open-Loop Model Structure of Propofol Delivery System (adapted from [7])

1.2.2 Open-Loop Model Identification

There is no single PKPD model that can predict the clinical effect of propofol on any given patient. This is evidently due to the fact that the clinical response of different patients to the anesthetic varies significantly with respect to demographics and drug tolerance, especially in children; this is

[4] The WAV_{CNS} index has the same significance as the DOH in terms of numerical value.

known as interpatient variability [1]-[7]. To account for this variability, the PKPD model parameters need to be identified based on clinical data obtained under the same surgical circumstances and for the same target populations for which the models are intended to be used [1],[4],[6],[7]. Multiple studies found in literature have performed PKPD model identification based on such data. Specifically, in [4] and [6], NeureSENSE measurements along with drug infusion profiles were recorded during 30 pediatric elective general surgeries where propofol, along with remifentanil, was administered manually by an anesthesiologist. In [1], the same was done for 44 adult subjects displaying significant variability.

In general, PK models are considered to be invariant with respect to interpatient variability, i.e., the relationship between $C_p(t)$ and the infusion profile $u(t)$ is given by a fixed-parameter transfer function with known parameters [1],[4],[6],[7]. Thus, the PD model parameters remain to be identified from the known $u(t)$ profile and the WAV_{CNS} measurements. In this respect, the PD model identification in the considered studies was performed in a similar two-step identification procedure. Firstly, the non-linear Hill function was omitted, and the FOTD model parameters were identified using the output-error method or standard least-squares estimation; specifically, the parameters k_d and T_d in equation (2) were identified from the patient's response to the known input $u(t)$, filtered through the PK model, and measured output WAV_{CNS} [1],[4],[6],[7]. In the second step, the non-linearity γ was identified by minimizing the residual errors resulting from the model fit obtained in the first step [1],[4],[6],[7]. The parameter E_0 required for the calculation of γ is obtained from the WAV_{CNS} by averaging over measurements made in the first instants of the drug induction; while EC_{50} can be obtained from step 1 of the identification [4],[6].

The PKPD model identification process involves several challenges that lead to loss of predictive accuracy [1],[4],[6],[7]. First, the inherent non-linearity of the model causes confusion in distinguishing between the effects of the time delay T_d and the non-linearity γ on the response [4],[6],[7]. The necessary linearization procedure performed to get around this difficulty thus tends to underestimate γ while overestimating T_d [4],[6],[7]. Another deficiency is that the synergistic effect of the remifentanil is not taken into account in the PKPD model, thus the identified parameters will be affected; from there stems the importance that these identified models be used under similar conditions where remifentanil is specifically administered with propofol [6]. As for the surgical disturbance $d(t)$ discussed before, we should note that the identified models were identified based on data from the propofol induction phase[5] only, when the surgical disturbance is minimal and thus does not affect model parameters [1],[4],[6],[7]. Another difficulty in system identification is the scarcity of available data given that it must be retrieved from actual surgery for specific target groups [6]. One last less concerning issue is sensor noise, but it is easily eliminated as it usually normally distributed with zero-mean and is eliminated by a low-pass filter [4],[7].

The system identification approach discussed in this section yields a set of identified PKPD models, namely one for each patient. For use in closed-loop control, the Hill sigmoids in these models are linearized around the DOH set point of 0.5 yielding a set of LTI plant models [1],[4],[6],[7]. From the latter, a single nominal model must be derived. Due to interpatient variability, this nominal model must be identified with care and will unavoidably involve some uncertainty [1]. Consequently, nominal model parameters are specified for specific age groups and under specific operating conditions [1],[4],[6],[7]. An interesting optimization approach for

[5] Induction is the phase when the patient is first put into anesthesia, surgical activity during this phase is minimal.

accounting for PKPD model uncertainty in deriving the nominal model is outlined in [1]. It involves expressing the PKPD model transfer function for each patient as a combination of the nominal transfer function and a certain deviation. The parameters of the nominal model are then optimized by minimizing the deviations between the fits resulting from the previously identified models and the nominal model representation; refer to [1] for further details.

1.2.3 Controller Design

Given an appropriately identified PKPD nominal model for the clinical effect of propofol on the patient, the loop can now be closed by designing a suitable controller that would handle the drug infusion profile based on comparing a reference DOH value set by the anesthesiologist with feedback from the DOH monitor. The controller must be designed so that the closed-loop system achieves a balance between performance and robustness, i.e. resilience against instability. However, in the setting of a medical application involving patients' lives, safety, and thus robustness, must be prioritized [1],[4],[7]. In particular, the DOH set point must be closely tracked by the control system since DOH overshoot is associated with apnea [4],[7]. On the other hand, slow propofol infusion is linked with pain and is not recommended [4],[7]. The right balance between robustness and performance is translated into the following typical step response[6] requirements (based on [1]):

- A Percent Overshoot (PO) that does not exceed 5%.
- A rise time T_r that ranges between 5 to 15 minutes.

[6] The DOH set point during propofol infusion is typically set to 50%, this corresponds to a step input.

In the studies reviewed in this paper, the selected controller type for the application at hand is a PID controller [1],[4]. Another controller type was proposed in [1], namely a CRONE controller, but we will restrict ourselves to the discussion of the PID controller only.

In [4], the PID controller parameters K_p, T_i and T_d were tuned using the linearized open-loop PKPD models in both the frequency and time domains. Robustness was assessed in the frequency domain as reflected by the achieved gain and phase margins while performance was evaluated in the time domain [4],[7]. The controller structure differed from a classical PID controller as the set point was excluded from the derivative path to avoid control signal spikes when the setpoint is suddenly changed and the derivative controller was initialized to a non-zero value resulting in a faster induction time [4],[7]. The final PID controller parameters were found after simulating the response of the closed-loop system for each of the study subjects and tuning for the best overall performance; these parameters were found to be $\{K = 5.4\, m, T_i = 255\, s, T_d = 33\, s\}$ [4],[7]. The proportional gain K is scaled by the patient's mass m, which is standard practice in PKPD modeling in pediatrics [4],[7].

[1] proposed a two-degree of freedom control scheme, it employs two controllers described by $G_{ff}(s)$ and $G_c(s)$ that are placed in the feedforward and feedback path respectively, as shown in Figure 3 below. The feedforward controller is PI type while the feedback controller is PID. This specific structure offers more freedom in tailoring each controller independently for one the two phases of the drug administration process, namely one for the induction phase and the other for the maintenance phase [1]. Another advantage is excluding the set point from the derivative control action which eliminates the risk of derivative kick [1]. Finally, to deal with uncertainty and reject disturbances, robust tuning was implemented by specifying a sensitivity function, which was maximized in order to reach a compromise between the closed loop robustness and performance

[1],[5]. Overall, the PID tuning scheme can be summarized by maximizing the integral gain k_i to minimize the integrated error and ensuring that the Nyquist curve of the closed-loop transfer function stays outside a circle of specific radius centered at -1 [1].

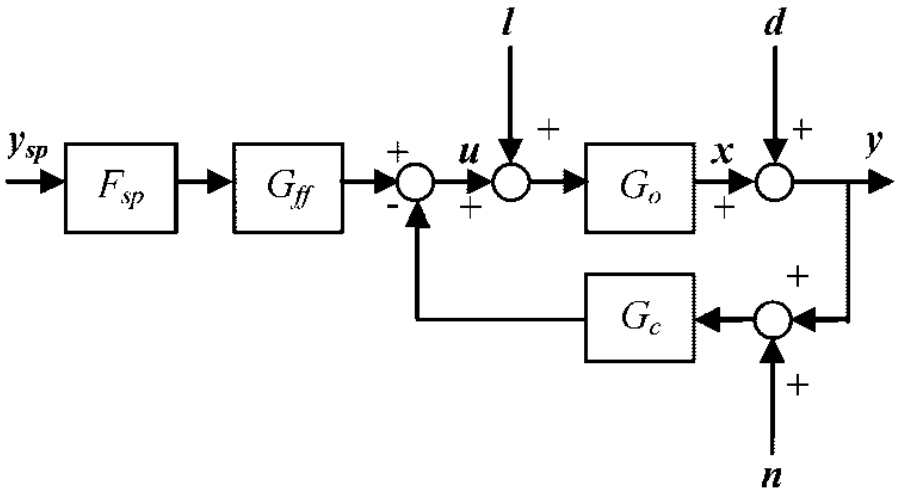

Figure 3: Closed-Loop Propofol Delivery System Structure (adapted from [1])

1.2.4 Advantages and Challenges

Several studies have shown, through clinical trials, that the implementation of an automated propofol delivery system is feasible and is indeed robust against interpatient variability and surgical disturbances, ensuring a safe and reliable drug administration process [1]-[7]. Moreover, it has been suggested that such closed-loop systems have the potential of guaranteeing a safer drug administration, reducing drug dosage, drug infusion time, patient wake up time, as well as workload on the anesthesiologist [1],[4],[7]. Nevertheless, many challenges must be overcome before these automatic systems become widely accepted for clinical applications. The main challenge being the issue of interpatient variability and the difficulty it poses when it comes to model identification as discussed before. Although the considered systems were tested in actual

trials, this validation remains restricted to a limited number of trials, which might not be enough to abide by medical safety standards. Furthermore, the advantages of closed-loop control over conventional methods need to be further emphasized by a larger number of validation clinical trials in order to convince the skeptical medical of their superiority.

2. System Identification

Our goal in this section is to describe the procedure of experimentally identifying a simplified open-loop model for the clinical effect of propofol. The identification task was performed in the idealized Simulink environment where the system to be identified was represented by a block implementing the system's unknown transfer function $G(s)$. The exact form of $G(s)$, i.e. the transfer function we attempted to estimate experimentally, is given by the following:

$$G(s) = Ke^{-T_d s}\frac{(s+z_1)(s+z_2)}{(s+p_1)(s+p_2)(s+p_3)(s+p_4)} \tag{4}$$

Where:

- $K = 1.4 \times 10^{-4}$
- $z_1 = 1.5 \times 10^{-3}; z_2 = 3.6 \times 10^{-5}$
- $p_1 = 2.87 \times 10^{-2}; p_2 = 7.75 \times 10^{-3}; p_3 = 2.85 \times 10^{-4}; p_4 = 8 \times 10^{-5}$
- $T_d = 8.5$

We shall now start by describing the methods followed to identify $G(s)$ in the Simulink setting to then present the findings of our system identification procedure and compare them with the actual model.

2.1 Methodology

2.1.1 General Approach

The system identification process was carried out based on the frequency response of the unknown system. That is, the unknown block implementing $G(s)$ was stimulated by a sinusoidal input of known frequency and amplitude, and the corresponding output was measured. The output signal was inspected after a certain amount of time has passed leaving room for the transients to decay, and the system to reach steady-state. The steady-state output turned out to be a sinusoid having the same frequency as the input signal. For convenience, the input sinusoid was chosen to have unity amplitude and zero phase. The input-output signals could then be plotted on the same graph, and the gain and phase shift between them were computed. The process was repeated for a set of logarithmically-spaced input frequencies[7] ranging from 10^{-6} to 1. The gain and phase shift measurements were then used to construct a bode diagram describing the unknown system's frequency response. The obtained bode diagram was later analyzed and used to identify the system's transfer function. The Simulink setup used to implement the described procedure is shown in Figure 4 below.

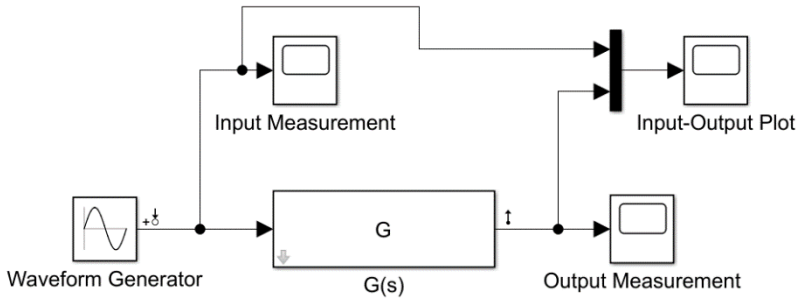

Figure 4: Experimental Simulink System Identification Setup

[7] The specified operating frequency range was specified after inspection of the output signal for various randomly chosen input frequencies.

2.1.2 Identification of $G(s)$

In our first system identification procedure where we attempted to estimate the exact transfer function $G(s)$, we used the built-in Frequency Response Estimation tool available in Simulink as part of the Control Design package. This tool implements the exact procedure outlined above in an automated manner; that is, it simulates the frequency response of a user-specified Simulink block by generating its bode plot. The input-output ports at which the simulator is to inject its input signal and measure the output signal were specified in the Simulink model, these ports are designated by the small symbols that can be seen in Figure 4 above. The type of input signals to be injected along with their parameters were then specified in the simulator's user interface; in our case, this consists of a stream of 60 sinusoidal signals with unit amplitude and logarithmically-spaced frequencies ranging from 10^{-6} to 1. The simulation was then launched, and its output was a bode diagram constructed from the gain and phase measurements made at the 60 different frequencies. A transfer function describing the unknown system was later identified from the obtained bode plot.

2.1.3 Identification of the Pade Approximation of $G(s)$

Another system identification task was performed for a first-order Pade approximation of $G(s)$. The later approximates the transport lag term $e^{-T_d s}$ by a first-order linear term. For a time delay $T_d = 8.5\ s$, the Pade approximation of $G(s)$ is given by:

$$G_{pade}(s) = K\frac{-s + 0.2353}{s + 0.2353}\frac{(s + z_1)(s + z_2)}{(s + p_1)(s + p_2)(s + p_3)(s + p_4)} \tag{5}$$

The same Simulink setup shown in Figure 4 was constructed, with the unknown block now implementing $G_{pade}(s)$ instead of $G(s)$. The identification process was done manually this time,

that is, the input sinusoids were injected one at a time and the output signals were measured. The input signals consisted of a set of 30 logarithmically-spaced input frequencies ranging between 10^{-6} and 1, the output was measured for each of these signals resulting in a total of 30 data points. In this approach, the magnitude and phase shift were calculated based on cursor measurements from the input-output scope shown in Figure 4, and the results were tabulated. The obtained data was then exported to MATLAB where a bode diagram was constructed for $G_{pade}(s)$; the transfer function could consequently be identified. We may now provide a sample calculation to illustrate our data collection method:

- For an input sinusoid having frequency of $\omega = 8 \times 10^{-4}\ rad/s$ and unit amplitude, we obtain the steady-state input-output plot shown in Figure 5.

- Using cursors, we measure the amplitude A of the output signal along with the time shift Δt between input and output. We find $A = 1.527$ and $\Delta t = -948\ s$.

- We then use these values to compute the magnitude and phase as:

  - $magnitude = 20 \log\left(\frac{A}{1}\right) = 20 \log(1.527) = 3.677\ dB$

  - $phase = \omega\, \Delta t = (8 \times 10^{-4})(-948) = 0.7584\ rad = -43.45°$

- This procedure is repeated for each of the 30 input frequencies obtaining enough data points allowing to construct an appropriate bode diagram.

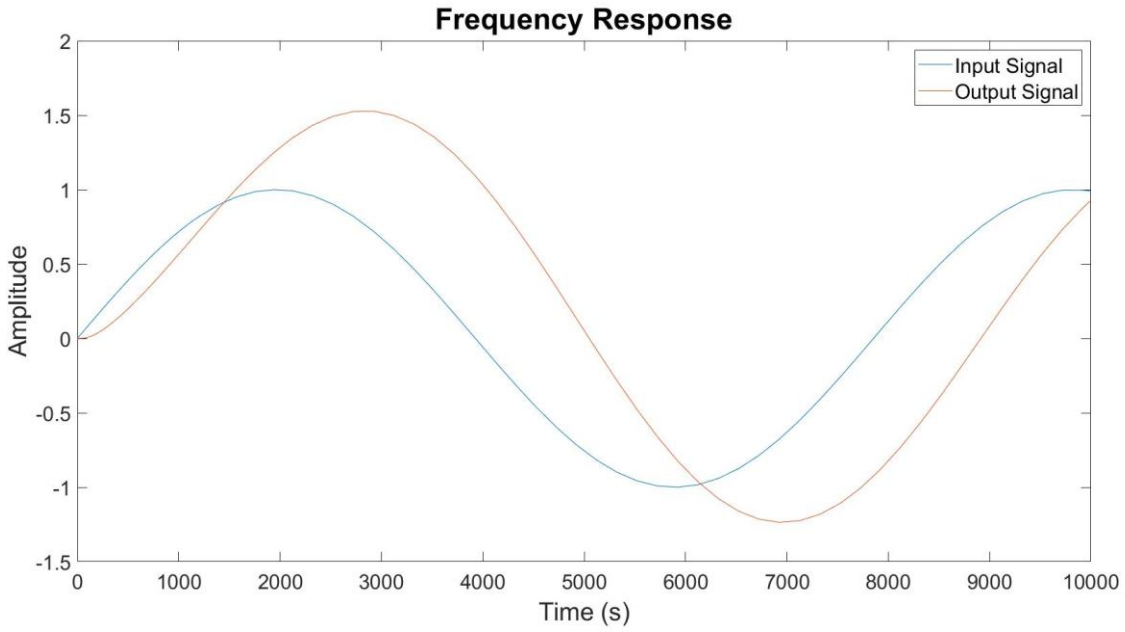

Figure 5: Frequency Response for an Input Frequency of $\mathbf{8 \times 10^{-4}}$ rad/s

2.2 Results

The system identification procedures described above yielded bode diagrams for both $G(j\omega)$ and $G_{pade}(j\omega)$. These diagrams were analyzed based on known frequency response behavior as reflected by asymptotic trends. The magnitude plot of $G(s)$ showed the presence of 6 first-order terms as indicated by a 20 $dB/decade$ change in slope at the identified corner frequencies; these terms were also found to correspond to 2 zeros and 4 poles. The system was identified to be of type 0 as the magnitude plot was found to have zero slope near $\omega = 0$ and thus the DC gain K was calculated from the value of the magnitude evaluated at $\omega = 0$. Figure 6 below shows the experimentally constructed bode plot of $G(s)$ on which asymptotes were drawn in order to locate the corner frequencies.

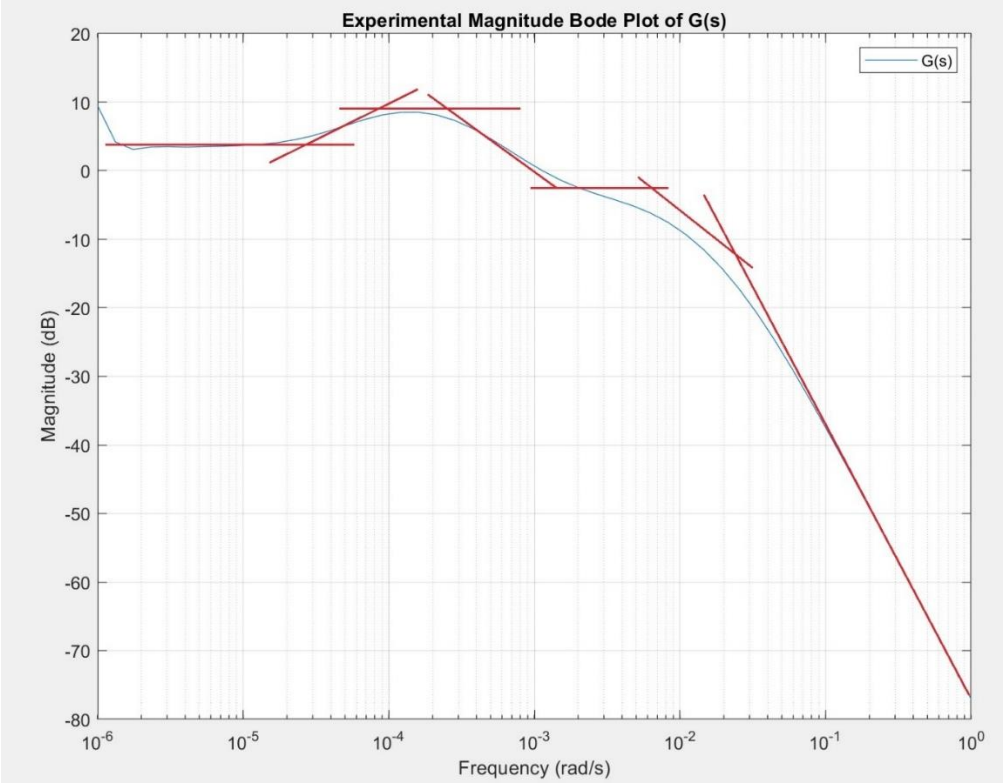

Figure 6: Experimental Bode Magnitude Plot of $G(s)$

The experimentally obtained phase plot showed a deviation from the characteristic phase plot of an LTI system having the corner frequencies identified above. This indicated the presence of a transport lag term in the system's transfer function. The lag term was identified by plotting the phase of the identified LTI transfer function (i.e. without the lag term) against the actual one. At a given frequency, the phase difference between the two plot corresponds to the phase lag induced by the transport delay, that is $\Delta\phi = \omega T_d$ at any frequency ω. The latter allowed the calculation of the time delay T_d. The analysis of the experimentally obtained bode plots thus yielded the following identified transfer function:

$$G_{id}(s) = (1.28 \times 10^{-4})e^{-8.51s}\frac{(s + 1.5 \times 10^{-3})(s + 3 \times 10^{-5})}{(s + 2.6 \times 10^{-2})(s + 7 \times 10^{-3})(s + 2.4 \times 10^{-4})(s + 8 \times 10^{-5})} \quad (6)$$

The identified model was found to closely fit the experimental data. Furthermore, it was found to be a good approximation of the exact transfer function $G(s)$ given by equation (4). This is illustrated in Figure 7 where it can be seen that the bode diagrams of the exact and experimentally identified transfer function are in agreement.

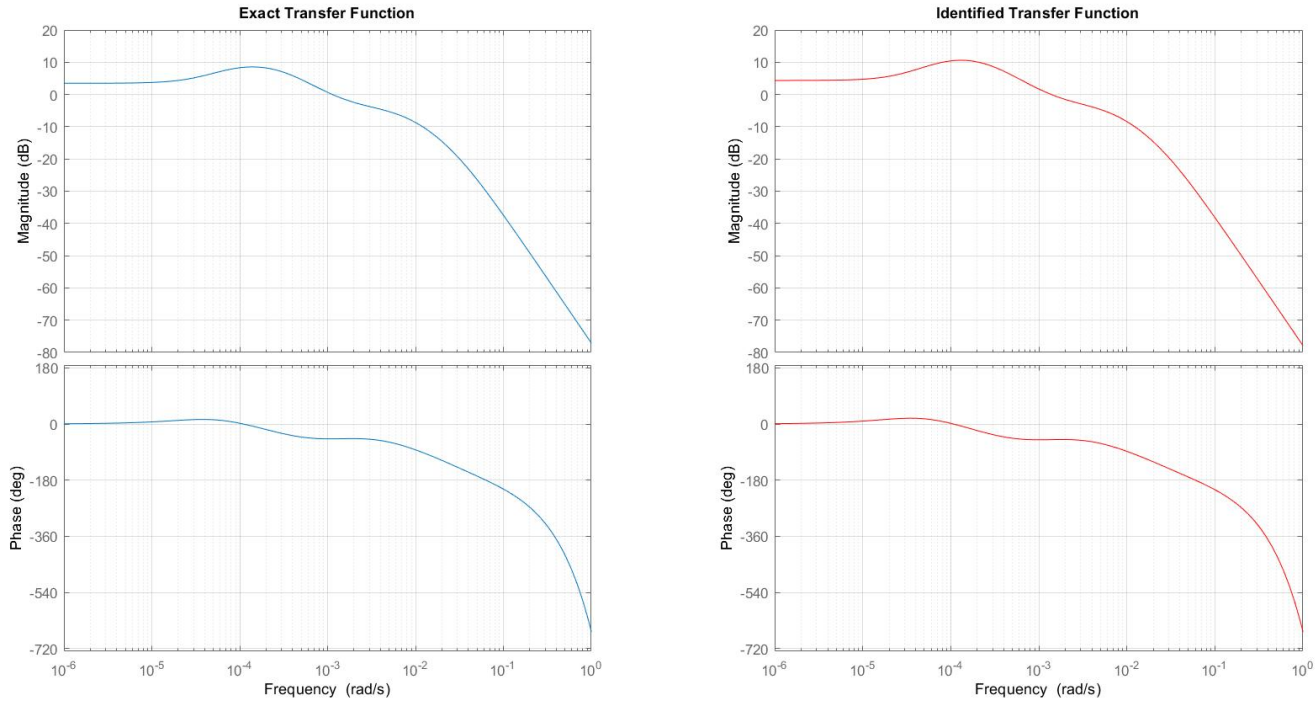

Figure 7: Comparison Between Exact and Experimental Bode Plots of $G(s)$

The experimentally obtained bode diagram of $G_{pade}(s)$ is shown in Figure 8 below. The obtained magnitude plot was found to be exactly the same as that of $G(s)$. This is expected as the Pade term is intended to approximate the transport lag, which does not alter magnitude characteristics. On the other hand, the obtained phase plot of $G_{pade}(s)$ differed from that of $G(s)$. In terms of system identification, $G_{pade}(s)$ was found to have the same components as $G(s)$, except that the transport lag term was replaced by a pole-zero pair located at around $\omega = \mp 0.23\ rad/s$ respectively. This was inferred from inspecting the phase plot of $G_{pade}(s)$ around that corner frequency.

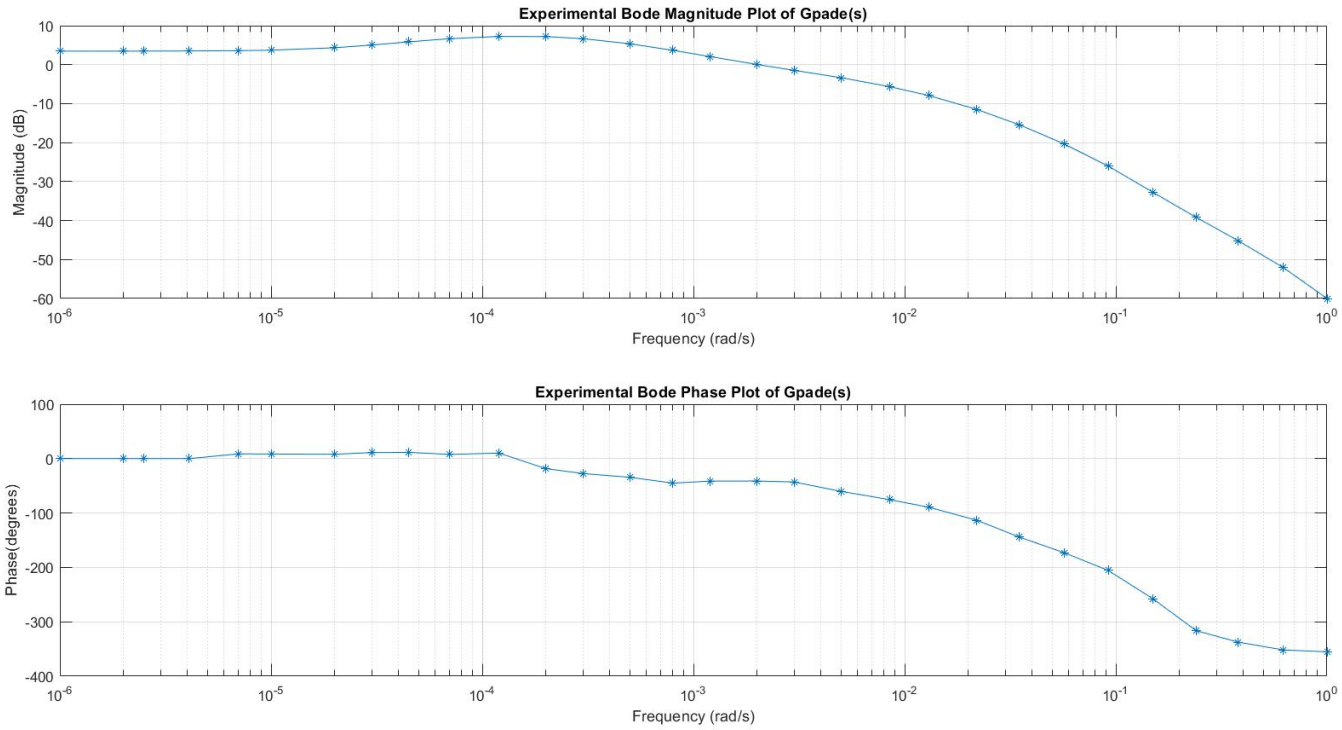

Figure 8: Experimental Bode Plot of $\boldsymbol{G_{pade}(s)}$

2.3 Higher Order Pade Approximations

2.3.1 Bode Plots

As mentioned before, approximating the transport lag term $e^{-T_d s}$ by a linear Pade term does not alter the magnitude plot of the transfer function. Mathematically, the latter is because the poles and zeros of the Pade approximant always come in pole-zero pairs of equal magnitudes and opposite signs, which, when applied to a certain transfer function, can effectively achieve a desired phase shift without altering its magnitude. Therefore, these poles and zeros can be chosen to produce an effect similar to that of the transport lag, which creates a phase shift that is proportional to frequency. Nevertheless, this structure has its limitations. We notice that, in terms of phase, the Pade approximation of $G(s)$ is able to track the exact function at low frequencies, but it diverges

from it at high frequencies. As the order of the Pade approximant is increased, the frequency range over which the approximation is valid increases. More specifically, we can notice that the phase plot of a Pade approximant of order n always asymptotically goes to a multiple of $-180°$, $-n180°$, as frequency increases; this is due to the inherent structure of the Pade approximant. The latter partially explains why the approximation gets better for higher order approximants and implies that the approximation will always breakdown at high enough frequencies. This discussion is best illustrated by comparing the bode diagrams of Pade approximation of increasing order to the exact transfer function $G(s)$. Refer to Figure 9 below where we can clearly see that the magnitude plot remains exactly the same for any approximation order whereas the phase plot converges to the exact one as the approximation order is increased.

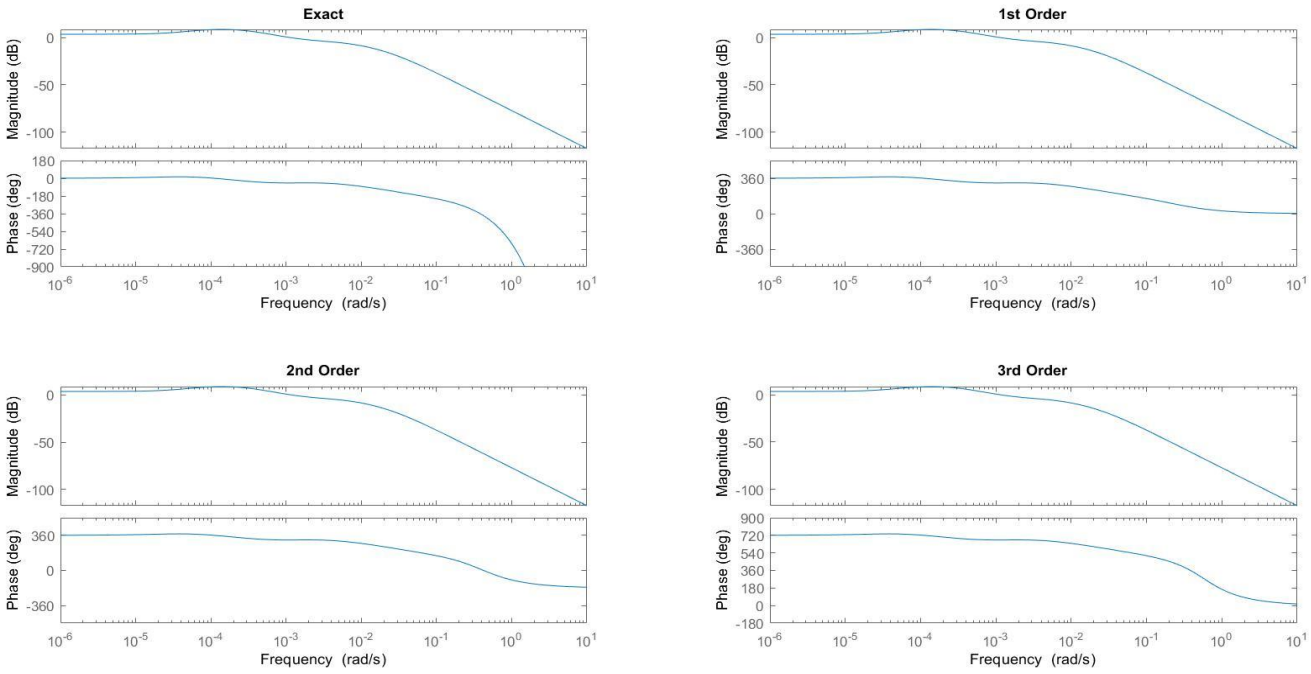

Figure 9: Bode Plots for Different Orders of the Pade Approximation[8]

[8] As can be seen in Figure 9, the phase plots for the different Pade approximations of $G(s)$ are shifted by multiples of $360°$; the axes were thus adjusted for better visualization.

2.3.2 Root Loci

Because of the non-linear transport lag term in the expression of $G(s)$, its root locus cannot be obtained using MATLAB. Instead, plots of the root loci of $G_{pade}(s)$ for different approximation orders are provided in Figure 10 below. As discussed before, an nth order Pade approximant consists of n pole-zero pairs of equal magnitude and opposite sign; in particular, the zeros are always positive while the poles are negative. Hence, $G_{pade}(s)$ will necessarily have open-loop zeros in the right half s-plane as can be seen in Figure 9. The presence of these zeros therefore implies that the system is non-minimum phase. So, being representative of the actual transfer function $G(s)$, the root loci of $G_{pade}(s)$ reflect the destabilizing effects of transport lag on the closed-loop system. In our case, the fact that the poles and zeros of $G(s)$ lie close to the origin further implies that the system is unstable for a large ranges of gain values. This calls for careful tuning and the addition of a controller to compensate for this deficiency.

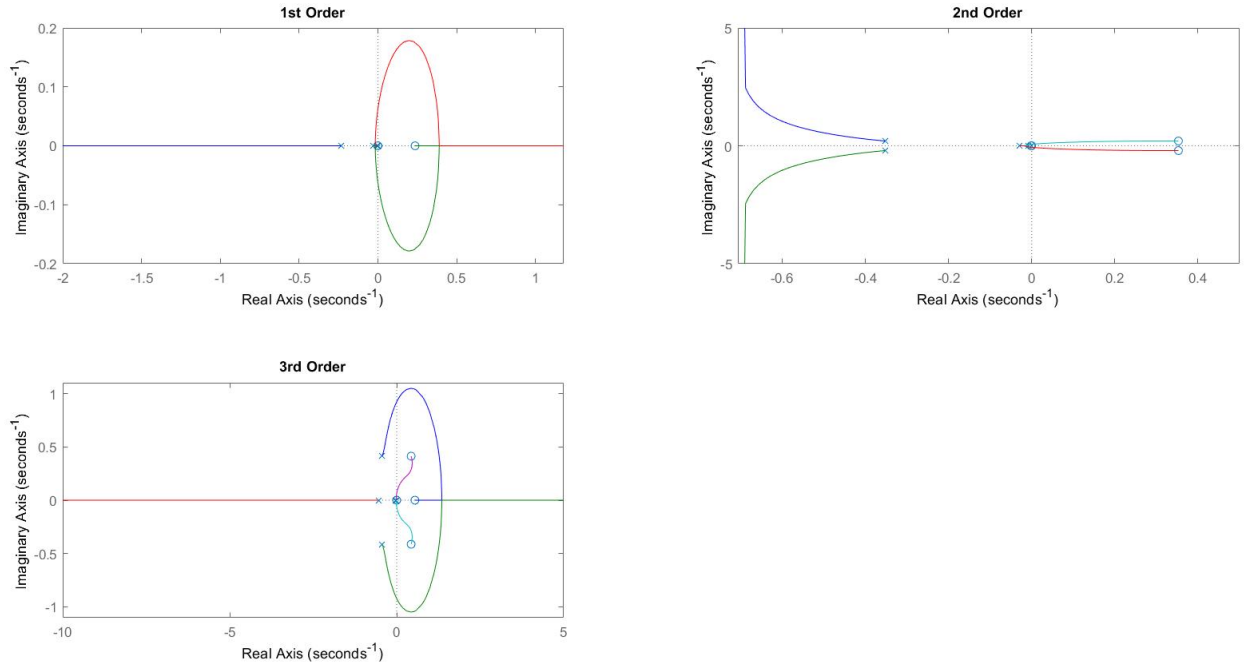

Figure 10: Root Loci for Different Orders of the Pade Approximation

2.4 Linearization of $G(s)$

Another way to obtain a linearization of $G(s)$ is using the MATLAB *linmod* command. The command works by linearizing each individual block in a given Simulink model then obtaining a transfer function for the now LTI system. In order to properly linearize the model using *linmod*, the transport lag needs to be implemented by a special Simulink block adapted for linearization called the *Switched Transport Delay* block. In this respect, the Simulink setup required for the proper use of *linmod* is shown in Figure 11 below, where $H1$ is the open-loop transfer function with the transport lag term omitted. It turns out that applying linmod on this model results in a linearized version of $G(s)$ that corresponds exactly to a second-order Pade approximation as illustrated by the bode plots in Figure 12.

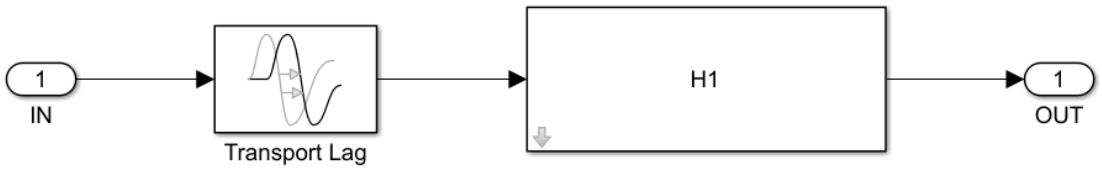

Figure 11: Simulink Setup for Linearization of $G(s)$ Using the linmod Command

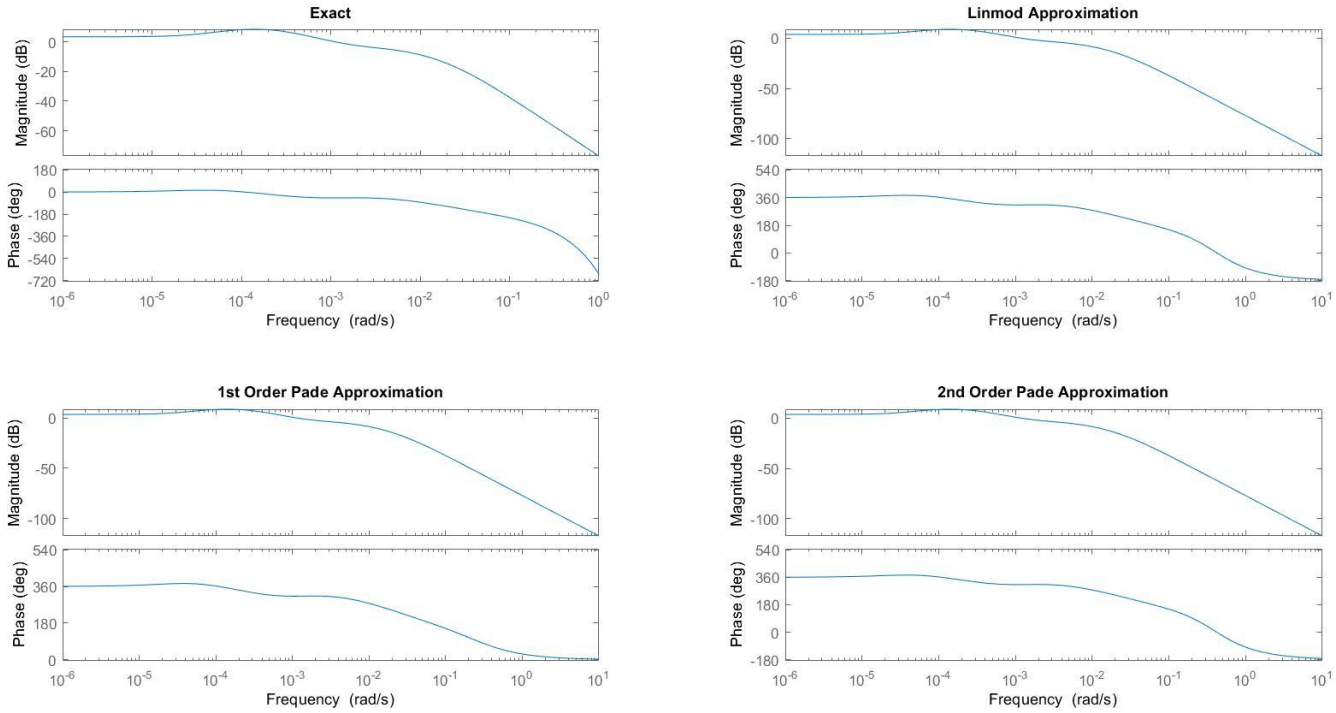

Figure 12: Bode Plots for linmod Linearization vs. Pade Approximations

3. Control System Design

In this section of the report, we will present two approaches for designing a controller suitable for use in closed-loop drug delivery systems. In particular, we consider two types of controllers, namely a Lag-Lead compensator and a PID controller. The controllers are to be designed such that the closed-loop system meets the following performance and steady-state error requirements when subject to a step input:

- Settling Time (2% criterion): $t_s = 20\ mins = 1200\ s$.
- Maximum Overshoot: $M_p = 3\%$.
- Steady-State Error: $e_{ss} = 2\%$.

For simplicity, we assume that the parameters of the open-loop transfer function given in equation (4) are modified as follows:

$$G(s) = Ke^{-T_d s}\frac{(s+z_1)(s+z_2)}{(s+p_1)(s+p_2)(s+p_3)(s+p_4)} \tag{7}$$

Where:

- $K = 1.7 \times 10^{-1}$
- $z_1 = 5 \times 10^{-2}; z_2 = 8 \times 10^{-2}$
- $p_1 = 10 \times 10^{-2}; p_2 = 3 \times 10^{-2}; p_3 = 4 \times 10^{-3}; p_4 = 0.5 \times 10^{-3}$
- $T_d = 8.5$

Furthermore, for the purposes of controller design, we may use the first-order Pade approximation of $G(s)$ instead of the exact transfer function. This is because the non-linear lag term poses problems when it comes to drawing root loci and other necessary computations in the design process.

3.1 Set Point

From the aforementioned transient response requirements, we determine the location of our desired dominant closed-loop poles denoted by the set point SP:

$$SP = (-3.333 \times 10^{-3}) \pm (2.986 \times 10^{-3})j \tag{8}$$

3.2 Angle of Deficiency

The first step in controller design is computing the angle of the complex open-loop transfer function evaluated at the set point and checking if it satisfies the angle condition. We find:

$$\angle G(SP) = 145.37° \neq 180° \tag{9}$$

Which implies that the angle condition is not satisfied, and thus the root locus of $G(s)$ does not pass through the set point. Hence a compensator is needed and must supply an angle of deficiency of:

$$\varphi = 34.63° \tag{10}$$

3.3 Lag-Lead Controller

The first controller considered is a Lag-Lead compensator. The Lead portion of that compensator was designed such that it supplies the required angle of deficiency computed above. The latter was designed by the bisection method yielding the following transfer function:

$$G_{c-Lead} = (6.62 \times 10^{-5}) \cdot \frac{s + 0.003522}{s + 0.005687} \tag{11}$$

The Lead compensator reshapes the root locus of $G_{pade}(s)$ making it pass through the set point, this ensures the satisfaction of the transient response requirements. However, the response still exhibits a steady state error of around 17.76%. This calls for the addition of a Lag compensator.

To design the Lag compensator, the static position error constant corresponding to a steady-state error of 2% was first determined to be $K_{p,des} = 49$. From that and the previous results, the zero to pole ratio of lag controller was found to be $\beta = 10.55$. Then, a value for the zero needed to be carefully chosen. Choosing this value too close to the origin would precisely achieve the desired steady-state error value along with locating the desired closed-loop poles at the exact set point. However, this would give rise to very slowly decaying exponentials in the transient response; these exponentials would dominate over our desired closed-loop poles resulting in a very lengthy settling time. On the other hand, locating this zero too far from the origin would alter the locations of the desired closed-loop poles, resulting in a dissatisfactory transient response performance. That been said, the location of the Lag compensator zero was tuned by trial and error in a way that resolves this tradeoff. The final form of the Lag compensator was thus found to be:

$$G_{c-Lag} = \frac{s + 4.7000 \times 10^{-4}}{s + 4.4568 \times 10^{-5}} \tag{12}$$

Verifying that:

$$-5° < \angle G_{c-Lag} = -3.96° < 0°$$

$$\left|G_{c-Lag}\right| = 0.93 \approx 1$$

We conclude that the design of this Lag compensator is satisfactory. This completes the design of the Lag-Lead network described by the transfer function below:

$$G_{Lag-Lead}(s) = (6.62 \times 10^{-5}) \cdot \frac{s + 0.003522}{s + 0.005687} \cdot \frac{s + 4.7000 \times 10^{-4}}{s + 4.4568 \times 10^{-5}} \quad (13)$$

The designed compensator was then tested in a closed-loop system with the exact transfer function $G(s)$. The step response of the closed-loop system was simulated (refer to Figure 13), and the resulting performance was characterized by the following:

- Settling Time (2% criterion): $t_s = 977.46\ s$.
- Maximum Overshoot: $M_p = 0.33\%$.
- Steady-State Error: e_{ss} =2%.

This performance is satisfactory with respect to the specified design requirements. Nevertheless, the location of the desired closed-loop poles was slightly altered by the Lag compensator and is now located at $s = (-3.264 \times 10^{-3}) \pm (2.684 \times 10^{-3})j$.

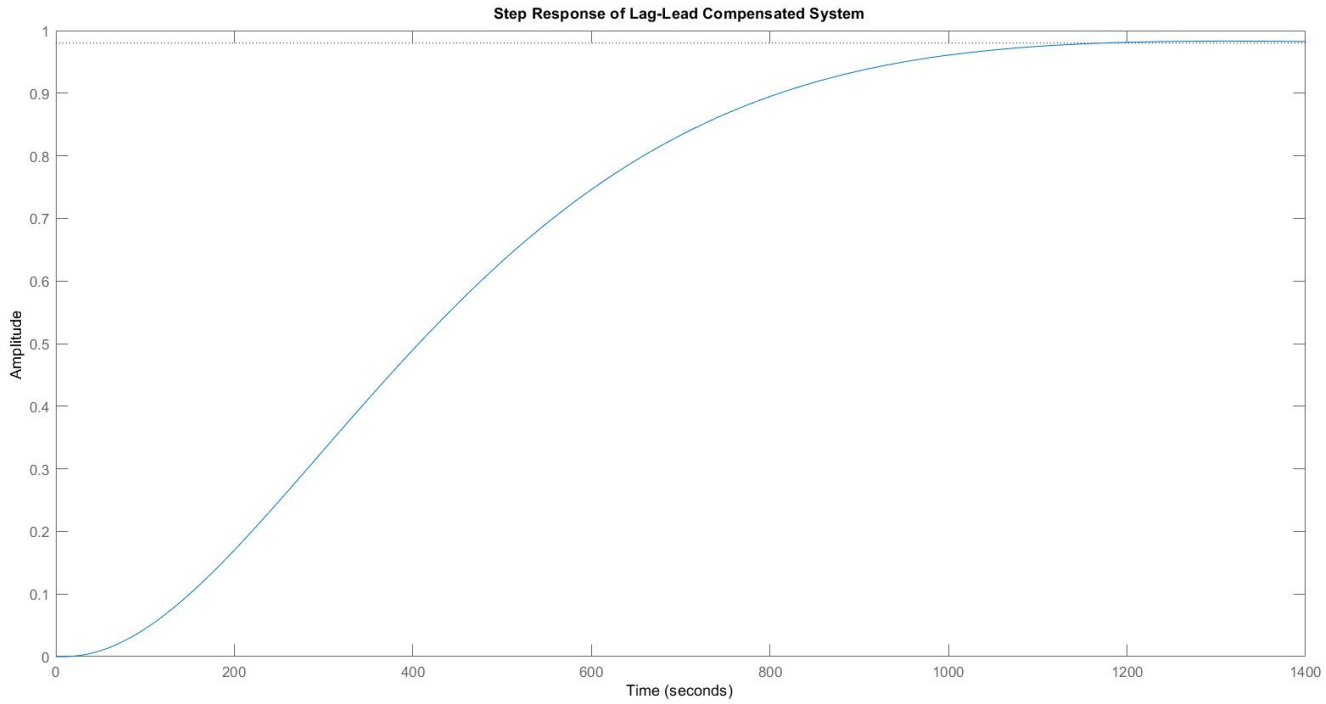

Figure 13: Step Response of the Lag-Lead Compensated Closed-Loop System

3.4 PID Controller

A PID controller was also designed for the same system. The PID controller's transfer function can be written as:

$$G_{PID}(s) = k_p + \frac{k_i}{s} + k_d = K_C \frac{(s+z_1)(s+z_2)}{s} \tag{14}$$

z_1 in the equation above was chosen so as to eliminate the plant's pole closest to the origin, $p_4 = 0.5 \times 10^{-3}$. z_2 was then found by requiring that the compensator supplies the angle of deficiency, that is setting $\angle G_{PID} = \varphi$ and solving for z_2. The gain K_c was found from the magnitude condition.

The obtained controller was then tested with $G(s)$ and the controller's parameters were slightly tuned to achieve the desired performance requirements. The final form of the controller was found to be:

$$G_{PID}(s) = (8.9871 \times 10^{-5}) + \frac{(4.1934 \times 10^{-8})}{s} + (0.0138)s \quad (15)$$

Being a type 1 system, the PID controller is expected to completely eliminate steady-state error for a step input. This was verified by simulating the closed-loop system (refer to Figure 14) and assessing its performance. The results were as follows:

- Settling Time (2% criterion): $t_s = 1115.20\ s$.
- Maximum Overshoot: $M_p = 2.84\%$.
- Steady-State Error: e_{ss} =0.24%.

As expected, the steady-state error was closed to zero. As for the transient response performance, it was found to abide by the design requirements.

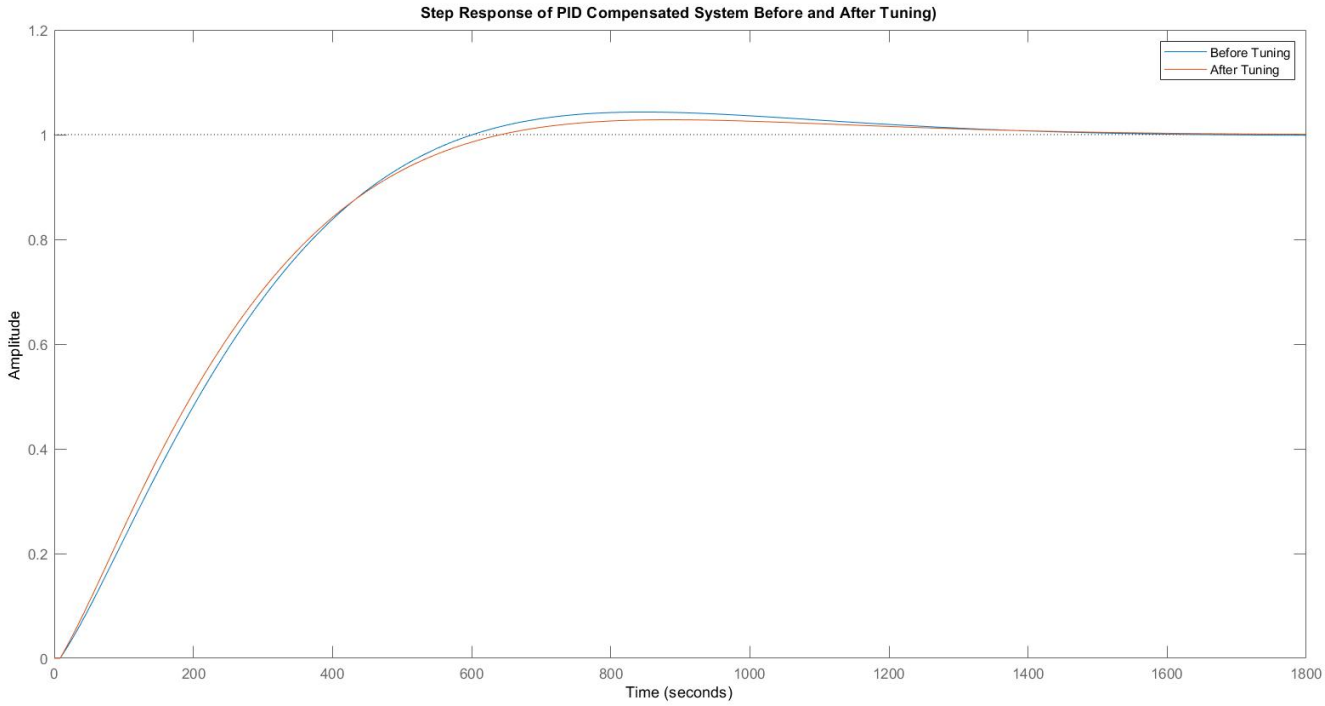

Figure 14: Step Response of the PID Compensated Before and After Tuning

3.5 Comparison to Ideal System

To assess the performance of the closed-loop control system with the two designed controllers, we compare the system's step response in each case to that of an ideal second-order system having its closed-loop poles at the desired location. Figure 15 below shows the simulated responses of the three considered systems. As can be seen, the PID compensated system exhibits the shortest rise time, whereas the Lag-Lead compensated system settles the earliest. The Lag-Lead compensated system also shows the smallest overshoot as compared to the other two systems which show almost the same overshoot. Finally, the most notable deficiency of the Lag-Lead compensator is its inability to eliminate steady-state error in contrast to the PID controller; this is due to the fact that the PID controller employs an integrator.

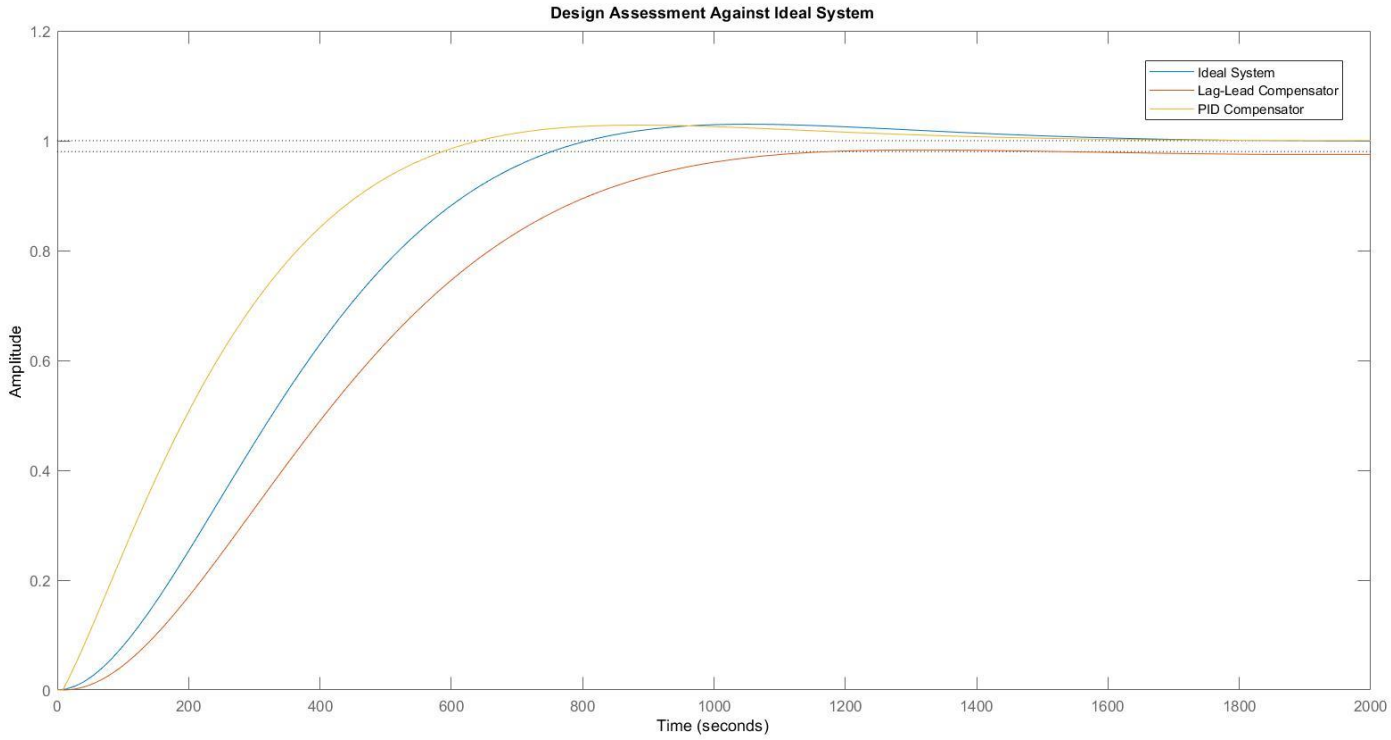

Figure 15: Response Comparison of Compensated System Vs. Ideal System

3.6 Bode Diagrams

A bode diagram was constructed based on the open-loop transfer function of the system with a Lag-Lead compensator then with a PID compensator, the plots are shown in Figure 16 below. As can be seen in the figure, the PID compensated system achieves higher stability margins. Specifically, the gain margin of the system with a PID controller was found to be of 38 dB as compared to 28.9 dB for the system with the Lag-Lead counterpart. In terms of phase margins, the PID compensator achieved a margin of 74.1 $degrees$ as opposed to 71.2 $degrees$ for the Lag-Lead compensator.

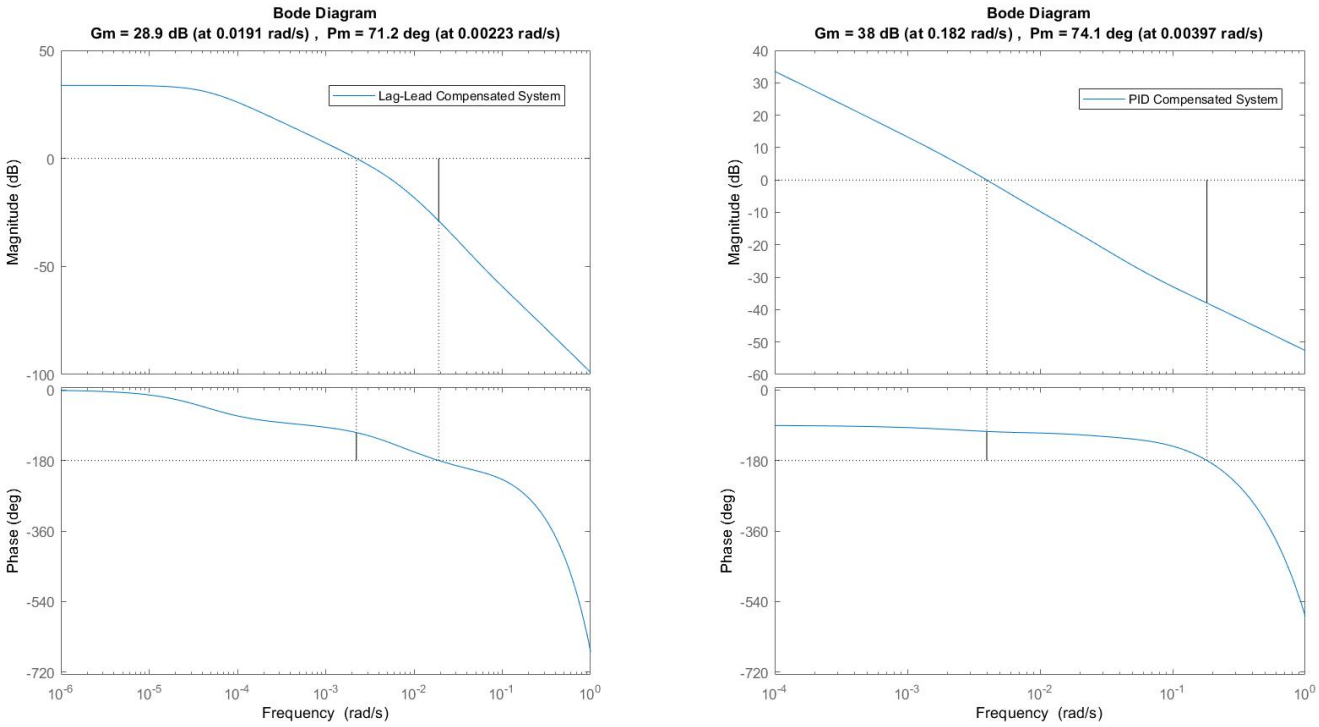

Figure 16: Bode Diagram of Compensated Systems

3.7 Actuating Signal

The actuating signal is the signal supplied by the compensator to the plant based on the computation of the error signal. By monitoring the latter through a scope on a built Simulink model for the compensated closed-loop system, we found that the actuating signal provided by the Lag-Lead compensator decays exponentially from a maximum value of $u_{max} = 6.6 \times 10^{-5}$ settling at a steady-state value of $u_{ss} = 0.8 \times 10^{-5}$. In contrast, the control signal provided by the PID compensator decays from a maximum value of $u_{max} = 1.4 \times 10^{5}$ to a steady-state value of $u_{ss} = 0.9 \times 10^{-5}$. The extremely large value of the actuation signal at the beginning of the simulation is attributed to the derivative controller since the reference input instantaneously jumps from 0 to 1 at $t = 0$. When adding a low-pass filter to the PID controller, this no longer happens, and the

actuation signal starts from $u_{max} = 1.4 \times 10^{-2}$. We can observe that although the PID control action starts at a much greater value than the Lag-Lead control action, it decays to the steady-state value in a much smaller time.

3.8 Effect of Non-Linearities: Saturation and Noise

Up until this point, our model for propofol infusion was tested in an ideal setup with no external disturbances affecting the system. In this section of the report, we will examine the effect of non-linearities on our system. In the Simulink environment, we will first subject our actuation signal to a saturation constraint, then we will add band-limited white noise to the feedback path of the closed-loop system.

3.8.1 Saturation Effects

In the Simulink model, a saturation block having upper and lower limits of 2×10^{-5} and 0 respectively was inserted between the compensator and the plant, and the model was simulated for a step input. The effects of the non-linear saturation block can be clearly visualized in Figure 17 below. Indeed, we can see that for both compensators, the system exhibits a significantly higher overshoot along with a slower response characterized by longer rise and settling times. These effects are due to the fact that the actuation signal saturates at 2×10^{-5}, which is below the maximum values u_{max} previously found with no saturation effects; this means that the actuation signal is below what is needed leading to a slower response and an error build-up later causing

overshoot. In our framework of a propofol delivery system, the saturation block can be thought of as modeling the propofol infusion pump which can provide a limited maximum infusion rate.

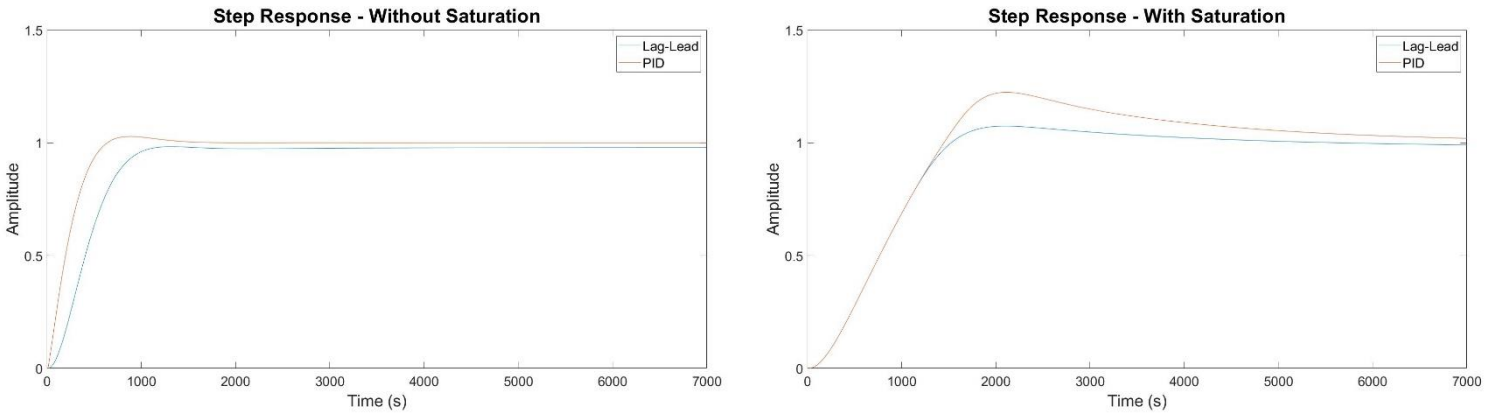

Figure 17: Effects of Saturation on System Response

3.8.2 Sensor Noise

Data corruption by noise is unavoidable in any practical application involving sensors. This is particularly concerning when we have derivative controller which is greatly affected by noise. This problem is usually resolved by equipping the D controller with a low-pass filter eliminating high frequency noise. For our purposes, noise was modeled by the Simulink *band-limited white noise* block; the noise sampling time was set to $1\ s$ and its power was varied between 0.001 and 0.1. The model was then simulated for the Lag-Lead compensator along with the PID without a filter and then with an added filter whose parameter N, corresponding to the low-pass filter's break frequency, set to 10^{-2} after consideration of the noise sampling time and the plant's dynamics. The obtained responses are shown in Figure 18 below. As expected, we can see that the filter limited the effect of noise on the output signal. Also, the Lag-Lead compensated system, which does not employ a D controller, did not face a noise problem. We can also observe that the addition of the filter caused the response to exhibit more overshoot and oscillations, this is because the filter attenuates the effect of the D controller. The latter poses a design tradeoff in tuning the parameter

N, a smaller value corresponds to better noise elimination at the expense of a more oscillatory response. This tuning should be done based on the noise power and sampling time, whereby a higher noise power corresponding to a greater destabilizing effect might require better attenuation characteristics and thus a smaller value of N.

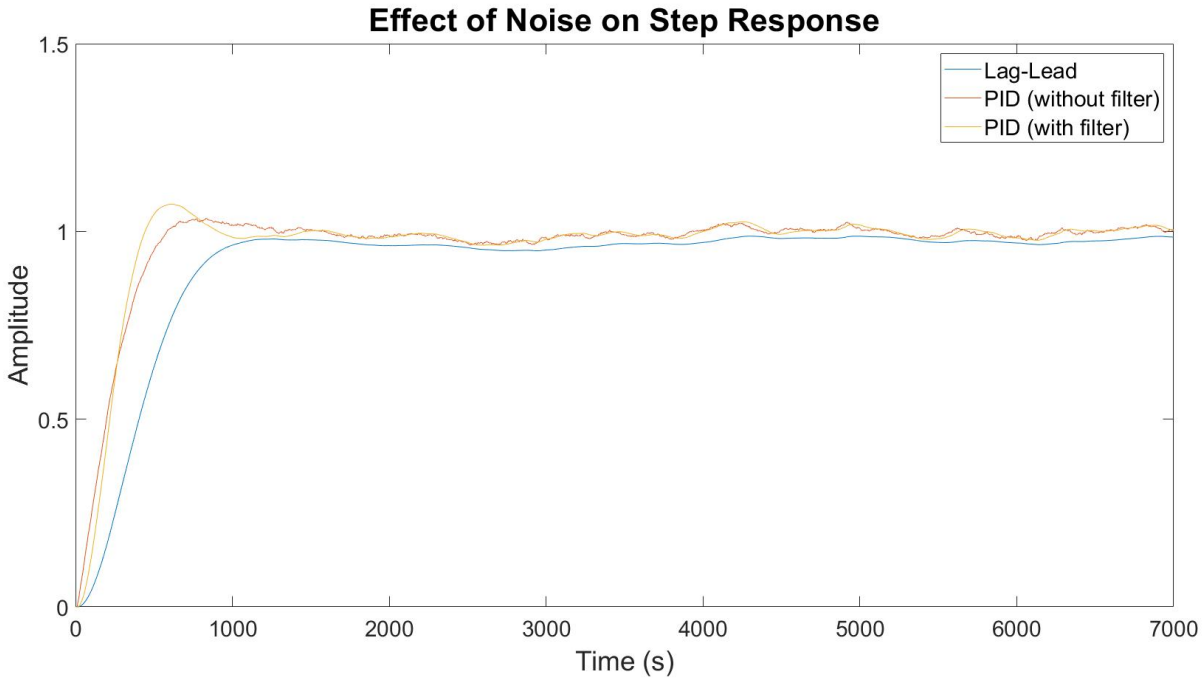

Figure 18: Effect of Noise on System Response (for N=0.01 and noise power set to 0.1)

Conclusion

The two design approaches presented in this paper proved to be adequate for developing a closed-loop control system for automatic propofol delivery as reflected by a satisfying transient and steady-state performance when subject to a step input. The latter was built upon a system identification scheme based on frequency response that allowed the determination of a representative open-loop model for the clinical effect of propofol. Furthermore, the compensated system was simulated in the presence of the non-linear effects of saturation and noise disturbances in an attempt to test it in a more realistic environment. The main challenge faced in the controller design process was the tradeoff, which appeared when designing the Lag compensator, between satisfying steady-state error requirements and transient response requirements. Finally, it is essential to note that the system was designed and tested in the idealized Simulink environment and is not appropriate for practical applications. Also, the considered model for the effect of propofol is a simplified one, a more representative model could consider the uncertainty imposed by interpatient variability among many other variables that should be accounted for if a truly robust controller is to be designed.

References

[1] Dumont, G. A., Martinez, A., & Ansermino, J. M. (2009). Robust control of depth of anesthesia. *International Journal of Adaptive Control and Signal Processing*, *23*(5), 435-454.

[2] Liu, N., & Rinehart, J. (2016). Closed-loop propofol administration: routine care or a research tool? What impact in the future?.

[3] Sartori, V., Schumacher, P. M., Bouillon, T., Luginbuehl, M., & Morari, M. (2006, January). On-line estimation of propofol pharmacodynamic parameters. In *2005 IEEE engineering in medicine and biology 27th annual conference* (pp. 74-77). IEEE.

[4] Soltesz, K., Van Heusden, K., Dumont, G. A., Hägglund, T., Petersen, C. L., West, N., & Ansermino, J. M. (2012). Closed-loop anesthesia in children using a PID controller: A pilot study. *IFAC Proceedings Volumes*, *45*(3), 317-322.

[5] Van Heusden, K., Ansermino, J. M., & Dumont, G. A. (2018). Performance of robust PID and Q-design controllers for propofol anesthesia. *IFAC-PapersOnLine*, *51*(4), 78-83.

[6] Van Heusden, K., Ansermino, J. M., Soltesz, K., Khosravi, S., West, N., & Dumont, G. A. (2013). Quantification of the variability in response to propofol administration in children. *IEEE Transactions on Biomedical Engineering*, *60*(9), 2521-2529.

[7] Van Heusden, K., Dumont, G. A., Soltesz, K., Petersen, C. L., Umedaly, A., West, N., & Ansermino, J. M. (2013). Design and clinical evaluation of robust PID control of propofol anesthesia in children. *IEEE Transactions on Control Systems Technology*, *22*(2), 491-501.